materials

Article

Dispersion of γ-Alumina Nano-Sized Spherical Particles in a Calamitic Liquid Crystal. Study and Optimization of the Confinement Effects

Sergio Diez-Berart [1,2,]*, **David O. López** [1,2], **Nerea Sebastián** [1], **María Rosario de la Fuente** [1], **Josep Salud** [2], **Beatriz Robles-Hernández** [1,2] **and Miguel Ángel Pérez-Jubindo** [1]

[1] Departamento de Física Aplicada II, Facultad de Ciencia y Tecnología, Universidad del País Vasco UPV-EHU, Apartado 644, Bilbao E-48080, Spain; E-Mails: david.orencio.lopez@upc.edu (D.O.L.); nerea.sebastian@ehu.es (N.S.); rosario.delafuente@ehu.es (M.R.F.); beatriz.robles@ehu.es (B.R.-H.); ma.perezjubindo@ehu.es (M.A.P.-J.)

[2] Grup de Propietas Físiques dels Materials (GRPFM), Departament de Física i Enginyeria Nuclear, E.T.S.E.I.B. Universitat Politècnica de Catalunya, Diagonal 647, Barcelona 08028, Spain; E-Mail: josep.salud@upc.edu

* Author to whom correspondence should be addressed; E-Mail: sergio.diez@upc.edu; Tel.: +34-934-054-107; Fax: +34-934-011-839.

Abstract: We report an experimental study on confined systems formed by butyloxybenzylidene octylaniline liquid crystal (4O.8) + γ-alumina nanoparticles. The effects of the confinement in the thermal and dielectric properties of the liquid crystal under different densities of nanoparticles is analyzed by means of high resolution Modulated Differential Scanning Calorimetry (MDSC) and broadband dielectric spectroscopy. First, a drastic depression of the N-I and SmA-N transition temperatures is observed with confinement, the more concentration of nanoparticles the deeper this depression is, driving the nematic range closer to the room temperature. An interesting experimental law is found for both transition temperatures. Second, the change in shape of the heat capacity peaks is quantified by means of the full width half maximum (FWHM). Third, the confinement does not noticeably affect the molecular dynamics. Finally, the combination of nanoparticles and the external applied electric field tends to favor the alignment of the molecules in metallic cells. All these results indicate that the confinement of liquid crystals by means of γ-alumina nanoparticles could be optimum for liquid crystal-based electrooptic devices.

1. Introduction

The importance of liquid crystals in the field of materials science is enormous, from theoretical and experimental reasons and, also, from the point of view of applications. Liquid crystal research covers many disciplines, from chemistry (design and synthesis), physics (fundamentals, models, characterization...), biology and medicine (many lyotropic liquid crystals are biocompatible and many biomolecules and macromolecules are mesogens), food and soap industries, thermal, mechanical, electronic and optical engineering (thermometers, biomechanic robots, displays, wave guides, lasers...) [1,2], *etc.*

Among all these industrial applications, liquid crystal-based electro-optical devices are largely spread and very well known. The duality of liquid-like fluidity and crystal-like anisotropy makes these materials ideal for such applications. On the one hand, the intrinsic dielectric and optical anisotropies imply a great variety of technical possibilities, as the compounds can be used in the construction of polarisers, filters, modulators, displays, *etc.* On the other hand, the fluidity of mesophases like the nematic (N) or smectic A (SmA) phases, among others, makes the molecules of the liquid crystal likely to orient *ad lib* by the application of small perturbations to the material (in form of electric or magnetic fields, simple chemical surfactants...). Putting these properties of liquid crystals together, the utility of such compounds in this field of technology is pretty obvious.

In order to design any electro-optical device based on liquid crystalline properties, optimizing not just the electrical and optical, but also the thermal properties of the mesogens, is one of the priorities. The importance of the thermal behavior lies in the fact that the device must be designed to work in a particular temperature range, the so called temperature window, depending on the application itself.

One simple way to tune the thermal, optical and electrical properties, improving some effects and reducing some others non-desired, is by means of confinement [3–37]. Quenched random disorder on liquid crystals may induce smooth and/or drastic variations in their physical properties and, therefore, an exhaustive study of these systems is of great importance. Furthermore, liquid crystals in a device are strongly perturbed by confining interfaces, which means that under adequate confinement techniques, we are able to study how the properties will behave in actual micro- or nano-sized devices, and we may, indeed, be hitting two targets with one shot.

In this work, we are studying the influence on the thermal, dielectric and dielectric properties of calamitic liquid crystals affected by the random disorder induced by the dispersion of nano-sizedγ-alumina particles, which are used for the first time for confining purposes. As shown recently [35], this kind of nanoparticles noticeably reduces the undesired ionic effects on liquid crystals, which goes in the good direction when the optimization of electrical properties is pursued. Furthermore, as we are about to demonstrate, they shift the phase transition temperatures down, in a very much drastic way as compared to other structures used for confinement purposes like, for example, Anopore membranes or Aerosil silica particles.

The material object of the present research is the butyloxybenzylidene octylaniline, hereafter refered as 4O.8, a smecto-nematogenic compound whose thermal properties in bulk [38,39], confined

in silica aerogel matrices [12] and confined under the dispersion of Aerosil particles [13,14] have been analyzed earlier. This is, however, the first time their dielectric properties, in bulk as well as under confinement, are reported, as it was claimed to be non-polar so far [13,38]. We show in this work that the molecule has a small (compared to common cyanobiphenyls) but measurable dipolar transversal moment, which induces a negative dielectric anisotropy.

The results presented in this manuscript, all for bulk and confined samples, are addressed in two parts, one for each of the studied properties: (1) We start with the calorimetric data, in which we can observe the deep depression in phase transition temperatures and the change in the shape of the heat capacity (C_p) peaks in the confined samples. Both effects are higher as the concentration of nanoparticles in the liquid crystal increases. A comparison between dispersions of γ-alumina and Aerosil nanoparticles is performed; (2) The behavior of the static and the complex dielectric permittivities, which allow us to interpret the molecular dynamics, is presented and discussed.

2. Results and Discussion

In order to check the influence of the random confinement on the analysed physical properties of the 4O.8 compound, we have prepared ten different samples: one bulk 4O.8 sample ($\rho_S = 0$), seven more with different concentrations of γ-alumina nanoparticles ($\rho_S = 0.01$ g cm^{-3}, $\rho_S = 0.05$ g cm^{-3}, $\rho_S = 0.13$ g cm^{-3}, $\rho_S = 0.17$ g cm^{-3}, $\rho_S = 0.19$ g cm^{-3}, $\rho_S = 0.23$ g cm^{-3} and $\rho_S = 0.28$ g cm^{-3}, where ρ_S accounts for density in grams of γ-alumina per cm^3 of 4O.8) and the last two with hydrophilic Aerosil dispersions ($\rho_{S,AS} = 0.05$ g cm^{-3} and $\rho_{S,AS} = 0.23$ g cm^{-3}). The main difference between the hydrophilic silica Aerosil and γ-alumina nanoparticles is that the formers are surrounded by OH radicals, whereas the latters are radical-free. In the case of hydrophilic Aerosil, when the weight concentration, $\rho_{S,AS}$, of these particles exceeds a certain threshold ($\rho_{S,AS} \sim 0.01$ g cm^{-3}), the OH groups tend to get attached forming hydrogen bonds, which induce the formation of thixotropic gelly structures. Depending on the concentration, these gels can be soft (0.01 g cm^{-3} < $\rho_{S,AS}$ < 0.1 g cm^{-3}) or stiff ($\rho_{S,AS} > 0.1$ g cm^{-3}), and the quenching of the mesogenic material becomes more pronounced as the concentration increases. Alumina nanoparticles, however, are not able to form these hydrogen bonds, as they are not coated with any functional group. They are spherical and have diameter lengths ranging between 3 and 30 nm, as can be observed from the transmission electronic microscopy (TEM) photo in Figure 1, being the average diameter about 15 nm.

Figure 1. Transmition Electronic Microscopy picture of the γ-alumina nanoparticles.
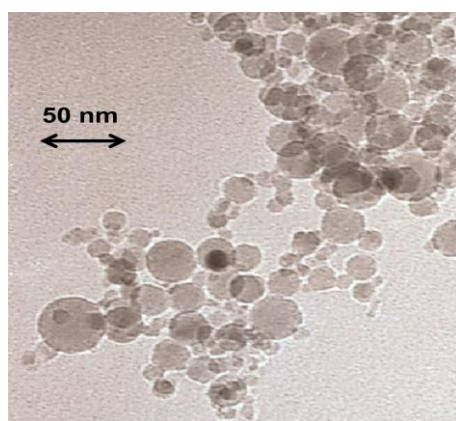
2.1. Thermal Analysis

The first issue to check is how the mesophases are affected by the dispersion of the nanoparticles. As mentioned above, 4O.8 is a smecto-nematogenic liquid crystal, and presents the following phase sequence on heating from room temperature: Crystal-Plastic Crystal-SmA-N-I. For the thermal analysis, we are focusing on the SmA-N and N-I phase transitions.

Figure 2 shows the excess heat capacity, ΔC_p, behavior as a function of temperature, for bulk 4O.8 and two of the γ-alumina dispersed samples ($\rho_S = 0.05$ g cm^{-3} and $\rho_S = 0.23$ g cm^{-3}), around the N-I phase transition. The SmA-N phase transition ΔC_p peaks of the same three samples are displayed in the inset of Figure 2.

Figure 2. Heat capacity data as a function of temperature near the N-I phase transition (and near the SmA-N phase transition in the inset) of the system 4O.8 + γ-alumina, for the samples with concentrations $\rho_S = 0$ (bulk, blue circles), $\rho_S = 0.05$ g cm^{-3} (green circles) and $\rho_S = 0.23$ g cm^{-3} (red circles). Dashed lines indicate the N-I (and SmA-N in the inset) transition temperatures for each of the samples.
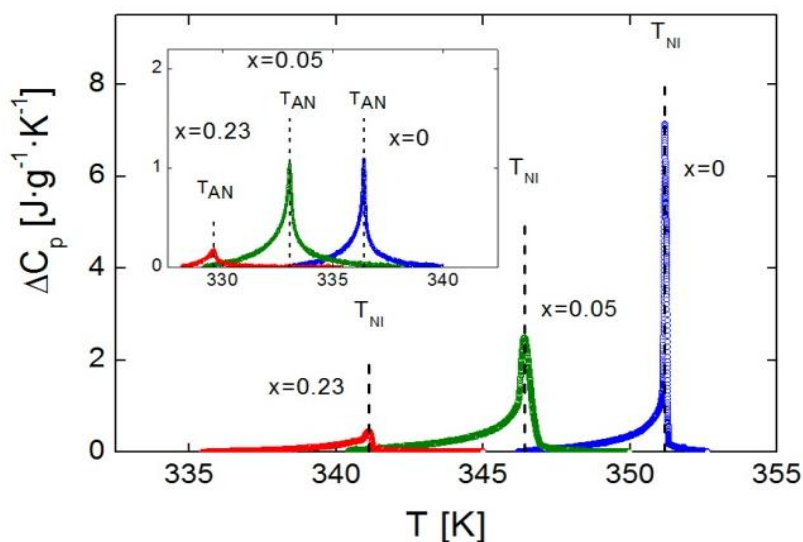
It can be observed that neither of the mesophases, SmA nor N, is suppressed by confinement. Furthermore, the more the concentration of nanoparticles, the more the transition temperatures are shifted down. It should be stressed that we are proving that the depression in transition temperatures is much more pronounced for confinement via γ-alumina than via Aerosil for the same concentration of nanoparticles, as shown in the values listed in Table 1. It can be seen how our data (in Aerosil) are quite in accordance with those from the work by Haga and Garland [13]. As it can be observed, and as a very interesting first result, moderate concentrations of γ-alumina nanoparticles are capable of shifting the SmA-N and N-I transition temperatures down to values around ten degrees below the bulk, and even more, while similar concentrations of Aerosil just make them decrease about two or three degrees.

Table 1. N-I and SmA-N phase transition temperatures and nematic range (NR) for the studied samples.

ρ_S (g cm^{-3})	T_{NI} (K)	T_{AN} (K)	NR (K)
0 (bulk 4O.8)	351.19	336.42	14.77
0.01	349.35 (−1.84)	334.86 (−1.56)	14.49
0.05	346.43 (−4.76)	333.34 (−3.08)	13.09
0.13	343.64 (−7.55)	331.34 (−5.08)	12.30
0.17	342.93 (−8.26)	330.95 (−5.47)	11.98
0.19	342.44 (−8.75)	330.34 (−6.08)	12.10
0.23	341.32 (−9.87)	329.86 (−6.53)	11.46
0.28	340.88 (−10.31)	329.26 (−7.16)	11.62
$\rho_{S,AS} = 0.05$	349.54 (−1.65)	334.64 (−1.78)	14.90
$\rho_{S,AS} = 0.23$	348.48 (−2.71)	333.89 (−2.53)	14.59

Figure 3 shows the dependence with concentration of the absolute value of the depression of the transition temperatures divided by the bulk transition temperature for the N-I (full circles) and SmA-N (empty circles) phase transitions. The experimental points for the studied concentrations can be fitted using the following equation (lines in Figure 3):

$$1 - \frac{T_{NI,\rho_s}}{T_{NI,bulk}} = \sqrt{a_{NI}\rho_s} \tag{1a}$$

$$1 - \frac{T_{AN,\rho_s}}{T_{AN,bulk}} = \sqrt{a_{AN}\rho_s} \tag{1b}$$

being T_{NI,ρ_s} the N-I phase transition temperature at the considered concentration, ρ_s; $T_{NI,bulk}$ the N-I phase transition temperature for the bulk, and a_{NI} the fitting parameter for the N-I phase transition, while T_{AN,ρ_s}, $T_{AN,bulk}$ and a_{AN} are corresponding parameters for the SmA-N phase transition. In the inset of Figure 3, we can see how the corresponding linear fittings are quite good. This result suggest that the depression of transition temperatures with concentration follows a monotonous behavior. However, when trying to obtain similar relationships with the Aerosil data this is not possible, as they clearly present a change of behaviour when passing from the soft-gel regime to the stiff-gel regime (~0.1 g cm^{-3}). These results seem to indicate that with γ-alumina nanoparticles there is not such a distinction between soft and stiff-gel regimes as with Aerosil, which is in accordance with the fact that the former do not have functional groups in the surface.

Another important outcome of this research is that the values of the fitting parameter *a* are 3.2×10^{-3} cm^3 g^{-1} for the N-I phase transition and 1.6×10^{-3} cm^3 g^{-1} for the SmA-N phase transition. There is a factor of about 2 between both transitions. The fact that the N-I transition temperatures become more affected than those of the SmA-N one, may indicate that, even if both transitions are weakly first order in nature, the latter is more continuous (more directed to second order). What is really impressive is the ratio of about 2 between both a_{NI} and a_{AN} parameters, which shall be object of further research.

Figure 3. Absolute value of the depression of the transition temperatures divided by the bulk transition temperature for the N-I (full circles) and SmA-N (empty circles) phase transitions. Straight and dashed lines indicate the fittings to Equations (1a,b), respectively. The inset shows the corresponding linear relationships coming from squaring Equations (1a,b).
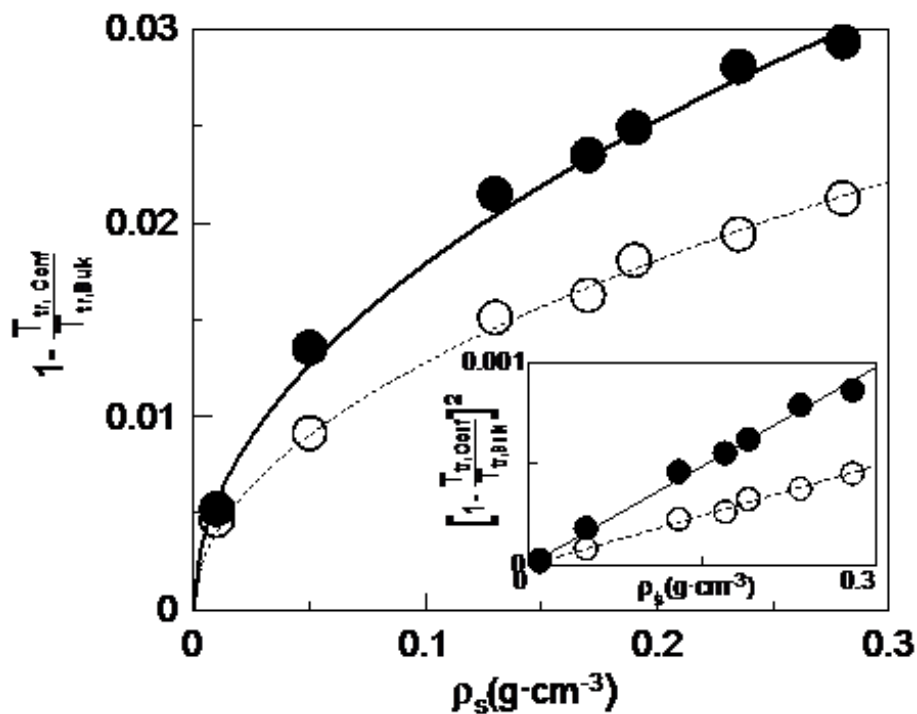
In addition to the change in transition temperatures, the influence of the confinement is remarkable in the shape and height of the C_p peaks in both the SmA-N and N-I phase transitions. As the concentration of nanoparticles increases, the C_p peaks become broader, rounded and shorter in height. This effect, that can be observed for the samples with $\rho_S = 0$, 0.05 and 0.23 g cm^{-3} in Figure 4a (N-I phase transition) and 4b (SmA-N phase transition), is qualitatively similar to what occurs in other types of liquid crystals under confinement [4,10,11,13,16,24,28,31,33]. A quantitative measure of the broadening of the peaks is done by means of their full width at half maximum (FWHM). The values of the FWHM in the N-I C_p peaks increase from 0.1 K in the bulk sample to ~0.3 K in the $\rho_S = 0.01$–0.19 g cm^{-3} samples, arriving up to ~0.5 K in the $\rho_S = 0.23$ g cm^{-3}, 0.28 g cm^{-3} samples. For the SmA-N peaks, FWHM goes from 0.2 K in the bulk to ~0.5 K in the confined samples. These values are similar to those corresponding to the dispersion of Aerosil nanoparticles in the same liquid crystal for small concentrations (soft-gel regime), as confirmed by the $\rho_{S,AS} = 0.05$ g cm^{-3} sample, where the FWHM is 0.3 K for the N-I peak and 0.5 K for the SmA-N one. Nevertheless, such values are much smaller than those for high concentrations (stiff-gel regime) of Aerosil in 4O.8, as for the $\rho_{S,AS} = 0.23$ g cm^{-3} sample, the FWHM of the N-I and SmA-N peaks are 0.8 K and 1.4 K, respectively. This confirms the fact that, at least, the γ-alumina particles do not form stiff-gels, as the Aerosil particles do. But the FWHM values are close to those samples comparable in concentration with Aerosil soft-gel regime ones, which means that FWHM measurements do not rule out the formation of soft-gels with γ-alumina nanoparticles. The question is, therefore, if γ-alumina nanoparticles can form any kind of soft-gel or similar, even if they cannot form hydrogen bonding networks.

Figure 4. Comparison of the excess heat capacity peak shapes near the (**a**) N-I and (**b**) SmA-N phase transitions for different concentrations of the 4O.8 + γ-alumina system: $\rho_S = 0$ (blue circles), $\rho_S = 0.05$ g cm^{-3} (green circles) and $\rho_S = 0.23$ g cm^{-3} (red circles). Dashed lines indicate the phase transitions.
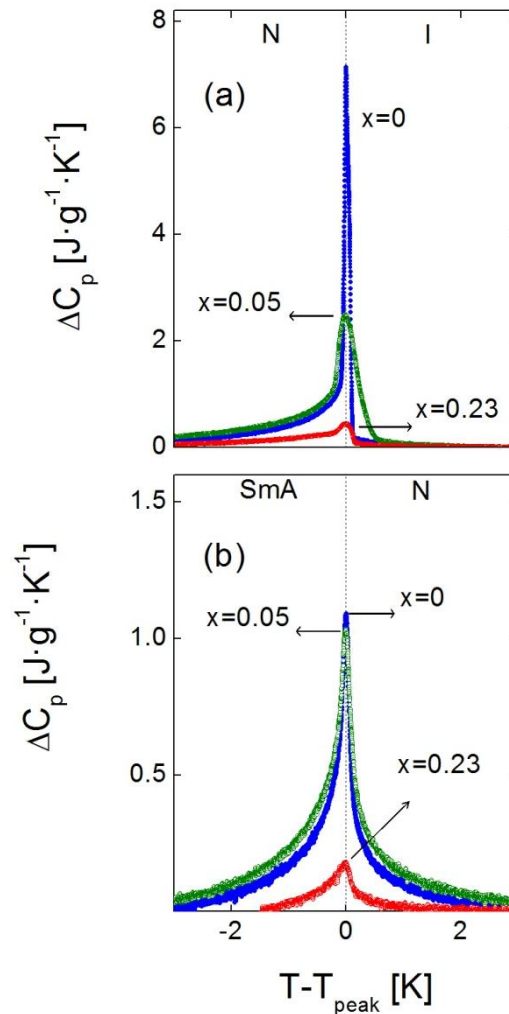
Regarding the experimental results about the drastic shifting down of transition temperatures together to the lower (compared to Aerosil) effect in the C_p peak-shapes for the confinement by means of γ-alumina nanoparticles, we may propose a possible explanation: Might be that when Aerosil particles form thixotropic gel structures small "islands" of liquid crystal are embedded inside the gel hollows. Such structures are much more uniform and homogeneous than the combination of the liquid crystal with dispersing γ-alumina particles, which might just act like "simple" impurities. The homogeneity of the LC + Aerosil structures could induce local anisotropic disordering, implying a drastic change with respect to the nature of the bulk liquid crystal, which is reflected in a marked variation in the nature of the phase transitions and, so, in the shape of the C_p peaks at the transitions. In the other hand, the LC + γ-alumina system simply lowers the transition temperatures but, at the same time, it just slightly changes the transitions' nature. The γ-alumina nanoparticles do not considerably alter the liquid crystalline structure, but they do introduce an isotropic disorder that just shifts the mesophases down in temperature. Such a distinction between gel structures and LC + impurities becomes clearer when particle concentration is high, which could explain why at low concentrations (soft-gel regime

for Aerosil) the C_p peak shapes in both N-I and SmA-N phase transitions are similar for both kinds of confinements. Anyhow, this remains an open question and more experiments must be performed in order to clarify and understand the behaviour of such confinements. Following this argument, we are now carrying on studies with γ-alumina nanoparticles dispersed in other kinds of liquid crystals [40].

Besides, the broadening of the C_p peaks means that the weakly first order phase transitions become even weaker with confinement and, eventually, might be driven to second order in nature [28,33]. Further exhaustive studies should be done in order to determine the critical behavior of these phase transitions, and see how it evolves with changing the concentration of nanoparticles, but such an analysis is beyond the scope of the present work.

2.2. Dielectric Analysis

First of all, it must be said that, in the dielectric measurements, the depressions in phase transition temperatures are not as pronounced as in the calorimetric ones. The difference in the samples themselves as well as the added interaction of the applied electric field, drastically change the transition temperatures behaviour with respect to the high resolution calorimetry experiments. Anyway, in this section we will just focus on the dielectric properties of the bulk 4O.8 and the influence of confinement in these properties alone. It should be stressed that such kind of studies are being performed for the first time in bulk 4O.8.

Several studies have claimed for the non-polarity of 4O.8 [13,38]. Nevertheless, the 4O.8 molecule has a mainly transverse dipole moment due to the imine group, as can be seen in Scheme 1.

Scheme 1. Butyloxybenzylidene octylaniline (4O.8) molecule.

$$C_4H_9\text{-}O \text{—}\langle\bigcirc\rangle\text{—} CH = N \text{—}\langle\bigcirc\rangle\text{—} C_8H_{17}$$
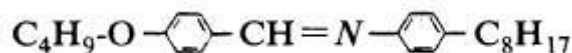
There is another transverse dipole due to the oxygen atom, that can be ruled out, in comparison with that of the imine group. Therefore, 4O.8 should present a negative dielectric anisotropy due to the mainly transverse dipole moment. In order to measure this response, measurements of the static and the complex dynamic dielectric permittivitty in the I, N and SmA phases have been performed, for bulk 4O.8 and for confined samples.

2.2.1. Static Dielectric Permittivity

As the perpendicular component of the static dielectric permittivity, $\varepsilon_\perp$, is higher than the parallel component, $\varepsilon_{||}$, the dielectric anisotropy of the molecules is negative ($\Delta\varepsilon = \varepsilon_{||} - \varepsilon_\perp$). This can be checked in Figure 5, were both components are presented *versus* T-T_{NI}, for two of the bulk, along with the static dielectric permittivity value in the isotropic phase. These measurements have been performed at 10 kHz, a frequency high enough to rule out the conductivity and ionic contributions and, at the same time, lower than that of the orientational contributions. The behavior of $\varepsilon_{||}$ and $\varepsilon_\perp$, for bulk as well as for confined samples, is the typical of calamitic liquid crystals with negative dielectric anisotropy [41]. Comparing to the bulk, the confined samples have a smaller dielectric anisotropy (in absolute value) in the N mesophase, which is nearly zero close to the N-I phase transition.

Figure 5. Static dielectric permittivity *vs.* temperature for the $\rho_S = 0$ (bulk) and $\rho_S = 0.28$ g cm^{-3} samples of the 4O.8 + γ-alumina system: Empty circles correspond to the isotropic phase; triangles correspond to the perpendicular component of the static dielectric permittivity in the mesophases, empty triangles for the $\rho_S = 0$ sample and full triangles for the $\rho_S = 0.28$ g cm^{-3} sample; squares represent the parallel component of the static dielectric permittivity in the mesophases, empty squares for $\rho_S = 0$ and full squares for $\rho_S = 0.28$ g cm^{-3}. The dashed line marks the N-I phase transition.
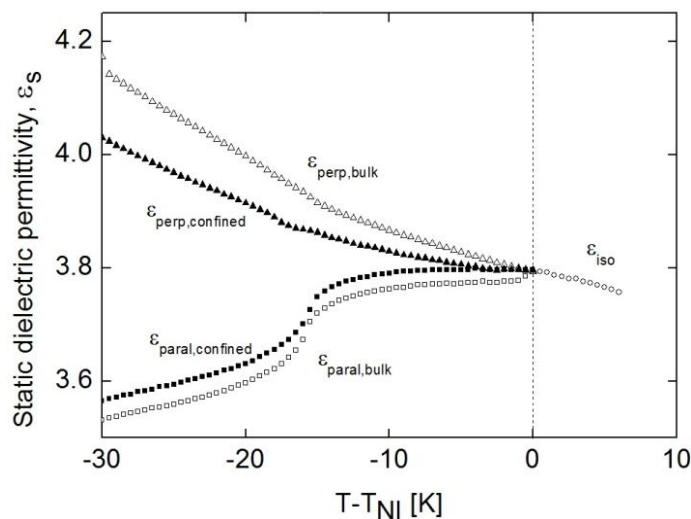

2.2.2. Molecular Dynamics: Relaxation Modes

Bulk Sample

Figure 6 shows both the real and imaginary parts of the complex dielectric permittivitty for bulk 4O.8, in both the I and N phases, the latter in a likely-planar alignment (molecules mainly parallel to the cell surfaces and perpendicular to the probing electric field). Spontaneously, the sample adopts a mixed alignment when placed into the metallic cell. When a bias DC field of 35 V is applied, the compound adopts a likely-planar alignment, as the material has a negative dielectric anisotropy. Any attempts to get the homeotropic alignment (molecules perpendicular to the cell surfaces and parallel to the probing electric field) was unfruitful. It can be observed the existence of two relaxation processes in both the I and N phases, the one at higher frequencies (around 1–10 GHz) with higher amplitude (about 3–5 times, depending on temperature) than the one at lower frequencies (1–10 MHz). Such a ratio in the strength of the modes is coherent with the fact that the dipolar moment is almost transverse (negative dielectric anisotropy). The low frequency mode (denoted as ω_1, from now on [42]) is due to the end-over-end rotations of the molecules around their short axis and the high frequency one (denoted as ω_2, from now on [42]) is due to the coupling of two types of molecular motions: rotations around their long axes and precessions around the nematic director. When cooling down to the SmA phase from the N, the behavior of the modes does not change significantly, being the spectra similar in both mesophases.

Figure 6. Frequency dependence of the real (full circles) and imaginary (empty circles) parts of the complex dielectric permittivity of the bulk 4O.8 (**a**) in the isotropic phase ($T = 353$ K) and (**b**) in the nematic phase ($T = 343$ K) in a likely-planar alignment. Black solid lines are fittings according to Equation (2). Red and blue lines represent deconvolution into the imaginary parts of the ω_1 and ω_2 modes, respectively. For simplicity, the direct current conductivity contribution (σ_{dc}) is not drawn, but is considered in the fitting procedure.
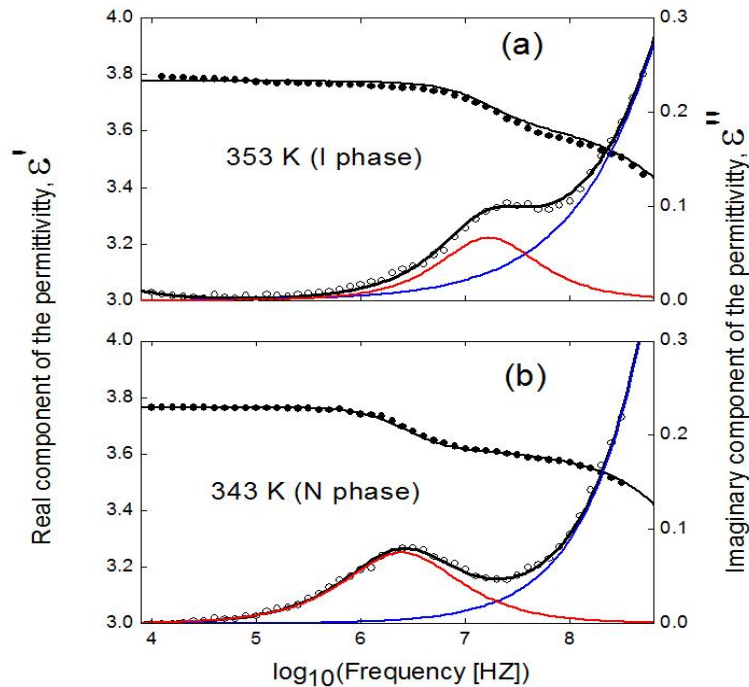
The experimental results of the complex dielectric permittivity, $\varepsilon(\omega)$, have been fitted through the empirical function:

$$\varepsilon(\omega) = \sum_k \frac{\Delta\varepsilon_k}{[1 + (i\omega\tau_k)^{\alpha_k}]^{\beta_k}} + \varepsilon_\infty - i\frac{\sigma_{DC}}{\omega\varepsilon_0} \tag{2}$$

where the summation is extended over the two relaxation modes, and each one is fitted according to the Havriliak-Negami function; $k = 1, 2$ are the different relaxation processs; $\Delta\varepsilon_k$ and τ_k are the dielectric strength and a relaxation time related to the frequency of maximum dielectric loss, respectively, of each relaxation mode; α_k and β_k are the parameters that describe the shape (width and symmetry) of the relaxation spectra; ε_∞ is the dielectric permittivity at high frequencies (but lower than those corresponding to atomic and electronic resonance phenomena) and σ_{DC} is the electric conductivity. According to the fits, ω_1 is a Debye relaxation mode ($\alpha = \beta = 1$). The high frequency mode (ω_2) lays in the brink of the frequency window and, therefore, the values coming from the fitting of such a mode must be taken with extreme caution. Although in Figure 6 the ω_2 mode is in the brink of the frequency window, it can be characterized at sufficiently low temperatures. This way, we have been able to fit the parameters of such a mode through Equation (2) at high temperatures, coming from lower temperatures and following a coherent behavior in their temperature dependences. Anyway, these fitting values must be taken with extreme caution, and we can temptativously say that ω_2 is a

Cole-Davidson mode ($\alpha = 1 \neq \beta$), with β ranging from 0.8 at high temperatures to 0.9 near the SmA-N phase transition.

The frequency dependence on temperature for both modes can be seen in the Arrhenius plot in Figure 7 (empty symbols). The presence of two relaxation modes in the isotropic phase is typical of materials with an anisotropic rotational diffusion tensor. The behavior of both modes is as expected for these kinds of molecular reorientations. The frequency jump for the ω_2 mode at the N-I phase transition is very smooth, and the activation energy of this relaxation is quite low, as expected for this kind of reorientations. On the other hand, ω_1 jumps down clearly in frequency when going from I to N and its activation energy is higher than that corresponding to the ω_2 mode. The validity of the fitting of ω_2, although limited, can be taken as optimal as its tendency is typical of these kind of relaxation modes in rod-like molecules [25,26,28,43], as can be seen from the Arrenius plot in Figure 7.

Figure 7. Arrhenius plot of the relaxation frequencies of the ω_1 (circles) and ω_2 (triangles) modes for the bulk 4O.8 (empty symbols) and $\rho_S = 0.28$ g cm^{-3} (full symbols) samples of the 4O.8 + γ-alumina system. Dashed lines indicate the N-I phase transitions for both samples.
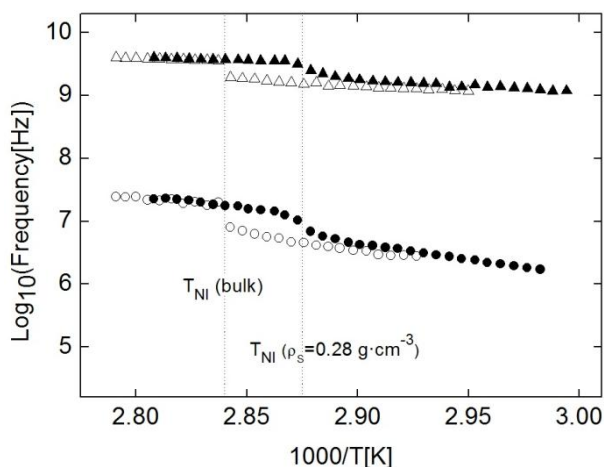
Confined Samples

The results of the confined samples (4O.8 + γ-alumina as well as 4O.8 + Aerosil) do not show noticeable differences with respect to the bulk ones, nor in amplitudes, neither in frequencies of the relaxation modes, but only the fact that they spontaneously adopt a planar alignment without a DC bias. In some cases, the spontaneous arrangement of calamitics in untreated metallic cells tends to be planar or nearly planar [43,44], though this is not always true and, sometimes, the cell surfaces must be treated with some surfactant in order to achieve the desired planar alignment of the molecules [25]. Fluidity of the nematic phase induces an average disorder of the molecules and, therefore, of the global nematic director, which translates in an inhomogeneous alignment of the sample, as is the case of the bulk 4O.8 sample. Nevertheless, the introduction of nanoparticles (γ-alumina as well as Aerosil) produces a decrease in fluidity and. Intriguingly, even if it induces random disorder, when combined with the applied electric field, it seems to increase the orientational order in a molecular planar alignment. Hence, the inhomogeneity within the metallic cell diminishes and the molecular

arrangement is more planar-like. If this were the case, it should induce the homeotropic molecular alignment in samples of liquid crystals with positive dielectric anisotropy confined by the dispersion of hydrophilic (polar) nanoparticles. We are currently trying to study this phenomenon with some liquid crystals with longitudinal net dipole moments.

With respect to the relaxation modes, the behavior is similar to that of the bulk sample, with the same ω_1 and ω_2 modes. As in the bulk, ω_1 is Debye-like and ω_2 is, temptatively, Cole-Davidson, with β ranging from 0.6 to 0.8 as temperature decreases. Full symbols in Figure 7 show the frequency dependence on temperature of both modes for the $\rho_S = 0.28$ g cm^{-3} sample. As it can be observed from this figure, the values are similar to those from the bulk sample, and this result can be reproduced for each of the studied samples. Such results mean that not only qualitatively, but also quantitatively, the dielectric behaviour of the planar samples is the same, irrespective of the given concentration (from $\rho_S = 0$ to $\rho_S = 0.28$ g cm^{-3}) and the nature (γ-alumina or Aerosil) of nanoparticles. As can be deduced from these results, fluidity differences between bulk and confined samples do not influence at all molecular reorientations.

3. Experimental Section

3.1. Preparation of the Materials

The pure 4O.8 compound was synthesized and purified at the Institute of Chemistry, Military University of Technology, Warsaw, Poland. Its purity was stated to be 99.6% and no further purification was made.

The alumina nanoparticles, in the γ-phase, were commercially obtained from Tecnan (Los Arcos, Spain) and their purity was claimed to be 99.995%. The density of the nanoparticles is about 3.65 g cm^{-3} and they have a surface area of about 110 m^2 g^{-1}. The particles, which are not coated with any functional group, are spherical and have diameter lengths ranging between 3 and 30 nm, as can be observed from the transmission electronic microscopy (TEM) photo in Figure 1, being the average diameter about 15 nm.

The silica spherical particles, of the type Aerosil 300, were commercially obtained by Degussa (Frankfurt, Germany). They are hydrophilic, with OH radicals in the surface and an average diameter of 7 nm. The quoted values of density and surface area are 2.6 g cm^{-3} and 300 m^2 g^{-1}, respectively. TEM measurements confirm that, as the γ-alumina particles, Aerosil particles present a polydispersive nature.

The dispersion of the nanoparticles in the pure compound was made mechanically, in an ultrasound bath in the isotropic phase (I) at temperatures slightly above the N-I transition temperature for the pure compound. The homogeneity of the mixtures was stated by the high resolution heat capacity measurements and the methodology of preparation was validated by comparison with bibliographical data for the Aerosil dispersions of the same liquid crystal [13].

3.2. Transmission Electronic Microscopy

A field transmission electronic microscope JEOL JSM-7001F was used. The sample was metallized with Pt-Pd, and the photo of Figure 1 was obtained at 200 K and 120 keV.

3.3. Heat Capacity Measurements

Static heat capacity data at constant pressure were obtained through the Modulated Differential Scanning Calorimetry (MDSC) technique via a commercial TA instruments Q-2000 (New Castle, DE, USA), for which extensive details can be found elsewhere [45]. Similar to an AC calorimeter, the MDSC technique, in addition to heat capacity data, simultaneously provides phase shift data (δ) that allow determining the phase coexistence region in weakly first order transitions. The experimental conditions were adjusted in such a way that the phase delay (δ) between the modulated heat flow (the response to the perturbation) and the induced temperature oscillations (perturbation) was nearly zero out of the phase transition, and the imaginary part of the complex heat capacity data vanished.

Typically, measurements were performed on heating from the crystal phase up to the isotropic phase; the temperature rate was 0.01 K min^{-1} with a modulation temperature amplitude (temperature oscillations) of $\pm$0.07 K and a period of 23 s.

3.4. Dielectric Measurements

Measurements of the static dielectric permittivity, ε_S, were performed using the HP 4192A impedance analyzer. We have used two different kind of square glass cells, depending on the desired alignment of the molecules with respect to the probing electric field. For measuring the parallel component of the static dielectric permittivity homeotropic alignment (molecules perpendicular to the cell surfaces) is required. Otherwise, for the study of the perpendicular component of the static dielectric permittivity, molecules must be in planar alignment (parallel to the cell surfaces). Both types of cells are from Instec (Boulder, CO, US), with an electrode surface of 1 cm^2 and thicknesses of 9 μm (homeotropic cells) and 8 μm (planar cells). The temperature control was made by a Linkam THMSG-600 hot stage and a Linkam TMS-94 temperature controller (Waterfield, Surrey, UK).

Measurements of the complex dielectric permittivitty were performed by means of two different equipments, depending on the analyzed frequency range. For radio frequencies (1 MHz to 1.8 GHz) the measurements were made by means of a HP 4291A impedance analyzer. For audio frequencies (1 kHz to 10 MHz) the HP 4192A impedance analyzer was used. The cell consists of two gold-plated brass electrodes (diameter 5 mm) separated by silica spacers, making a plane capacitor of about 50 μm thick. A modified HP 16091A coaxial test fixture was used as the sample holder. It was held in a cryostat made by Novocontrol (Hundsangen, Germany), and both temperature and dielectric measurements were computer controlled. Additional details of the experimental technique can be found somewhere else [43,45,46]. Dielectric measurements were performed on cooling with stabilization at different temperature steps and a temperature control on the order of 20 mK.

4. Conclusions

In the present work, we have presented a high resolution calorimetric and dielectric study both in 4O.8 bulk and in confined samples of γ-alumina nanoparticles dispersed in 4O.8.

The dispersion of γ-alumina nanoparticles in 4O.8 shifts downwards both N-I and SmA-N phase transition temperatures. The higher the concentration of nanoparticles, the lower the transition temperatures are with respect to the bulk. This effect is typical of confined systems, but in this case the

decrease of the phase transition temperatures is much more pronounced than with any other type of confinement studied so far. For comparable concentrations of nanoparticles (γ-alumina and Aerosil), the T_{NI} shifts down three times more (low concentrations) and four times more (high concentrations) in the case of γ-alumina than in the case of Aerosil. Regarding the T_{AN}, the shifting down from the bulk is about twice more (low concentrations) and three times more (high concentrations).

An important experimental result to compare confinement by means of γ-alumina or Aerosil is the possibility of fitting data with γ-alumina to Equations (1a,b), which cannot be done for Aerosil data, in which there is a clear change of behavior. This suggests that γ-alumina nanoparticles, unlike Aerosil, do not present two different regimes, *i.e.*, a soft-gel regime below concentrations of about 0.1 g cm^{-3} and a stiff-gel regime above. The relationship of these fittings between both N-I and SmA-N phase transitions is really intriguing as there is a correspondence of about 2:1 between the a_{NI} and the a_{AN} fitting parameters. Additional studies should be undertaken.

The other thermal effect caused by the confinement is the change in the shape and height of the heat capacity peaks at phase transitions. In the studied case, this change of shape (reflected as a brodening) is not as noticeable as for the confinement by means of Aerosil. The values of the FWHM of the C_p peaks of the 4O.8 + γ-alumina are similar than those of Aerosil dispersions for the so-called soft-gel regime ($\rho_S < 0.1$ g cm^{-3}), but are much smaller for the stiff-gel regime ($\rho_S > 0.1$ g cm^{-3}). In summary, γ-alumina nanoparticles introduces a disorder in the compound, *i.e.*, it favours the more disordered phases with respect to the more ordered ones, as observed by a notable lowering of both N-I and SmA-N transition temperatures. Althoug this also happens by means of Aerosil dispersion, with the γ-alumina it is much more pronounced. At the same time, confinement by means of γ-alumina does not affect the nature of the phase transitions as much as Aerosil particles do for high concentrations ($\rho_S > 0.1$ g cm^{-3}). This seems to indicate that the γ-alumina nanoparticles, at least do not form stiff-gels, like the Aerosil does.

The most noticeable change in the dielectric results consequence of the confinement is that the dielectric anisotropy is less negative than in the bulk. The dynamic dielectric properties are similar for bulk and confined samples, presenting two relaxation modes (reorientations around short and long molecular axes) whose frequencies do not depend on nanoparticles concentration whatsoever. There is, nevertheless, one interesting influence of the γ-alumina (and Aerosil also) particles, which is the induced ordering of the molecules facilitating planar configurations in metallic samples, when bulk 4O.8 adopts an inhomogenous fashion.

Finally, we would like to say that the 4O.8 + γ-alumina system could be an optimal candidate for electro-optical applications, for the following reasons: (1) the nematic range can get closer to room temperature with concentration of nanoparticles and, so, more accessible for device applications; (2) dielectric properties do not suffer significant changes due to confinement, which is interesting in the meaning that molecular dynamics is not slowed down and electro-optical response is, therefore, fast enough for switching applications; (3) it seems that γ-alumina nanoparticles improve the molecular orientational ordering with the dipolar moment parallel to the applied electric field.

Acknowledgments

Author Contributions

Sergio Diez Berart and David O. López have planned the work. SDB and Josep Salud have made the confined samples. DOL and JS have performed high resolution calorimetric measurements. María Rosario de la Fuente and Miguel Ángel Pérez Jubindo planned the dielectric measurements. SDB, Nerea Sebastián and Beatriz Robles Hernández performed and analyzed dielectric measurements. SDB has written the paper.

Conflicts of Interest

The authors declare no conflict of interest.

References

1. Sage, I.C.; Crossland, W.A.; Wilkinson, T.D.; Gleeson, H.F.; Leigh, W.J.; Workentin, M.S. Applications. In *Handbook of Liquid Crystals*, 1st ed.; Demus, D., Goodby, J.W., Gray, G.W., Spiess, H.W., Eds.; Wiley-VCH: Weinheim, Germany, 1998; Volume 1, pp. 731–895.

2. Blunk, D.; Praefcke, K.; Vill, V.; Fairhurst, C.; Fuller, S.; Gray, J.; Holmes, M.C.; Tiddy, G.J.T.; Hoffmann, S.; Zugenmaier, P. Amphiphilic Liquid Crystals. In *Handbook of Liquid Crystals*, 1st ed.; Demus, D., Goodby, J.W., Gray, G.W., Spiess, H.W., Eds.; Wiley-VCH: Weinheim, Germany, 1998; Volume 3, pp. 303–482.

3. Bellini, T.; Clark, N.A.; Muzny, C.D.; Wu, L.; Garland, C.W.; Shaefer, D.W.; Oliver, B.J. Phase-behavior of the liquid-crystal 8CB in a silica aerogel. *Phys*. *Rev*. *Lett*. **1992**, *69*, 788–791.

4. Iannacchione, G.S.; Finotello, D. Calorimetric study of phase transitions in confined liquid crystals. *Phys*. *Rev*. *Lett*. **1992**, *69*, 2094–2097.

5. Iannacchione, G.S.; Crawford, G.P.; Zumer, S.; Doane, J.W.; Finotello, D. Randomly constrained orientational order in porous glass. *Phys*. *Rev*. *Lett*. **1993**, *71*, 2595–2598.

6. Iannacchione, G.S.; Mang, J.T.; Kumar, S.; Finotello, D. Surface-induced discrete smectic order in the isotropic phase of 12CB in cylindrical pores. *Phys*. *Rev*. *Lett*. **1994**, *73*, 2708–2711.

7. Wu, L.; Zhou, B.; Garland, C.W.; Bellini, T.; Shaefer, D.W. Heat-capacity study of nematic-isotropic and nematic-smectic-A transitions for octylcyanobiphenyl in silica aerogels. *Phys*. *Rev*. *E* **1995**, *51*, 2157–2165.

8. Iannacchione, G.S.; Crawford, G.P.; Qian, S.; Doane, J.W.; Finotello, D.; Zumer, S. Nematic ordering in highly restrictive Vycor glass. *Phys*. *Rev*. *E* **1996**, *53*, 2402–2411.

9. Qian, S.; Iannacchione, G.S.; Finotello, D. Critical behavior at the smectic-A to nematic transition confined to a random network. *Phys*. *Rev*. *E* **1996**, *53*, R4291–R4294.

10. Zhou, B.; Iannachionne, G.S.; Garland, C.W.; Bellini, T. Random-field effects on the nematic-smectic A phase transition due to silica aerosil particles. *Phys. Rev. E* **1997**, *55*, 2962–2968.

11. Kutnjak, Z.; Garland, C.W. Calorimetric study of phase transitions for butyloxybenzylidene octylaniline in silica aerogels: Static and dynamic behavior. *Phys. Rev. E* **1997**, *55*, 488–495.

12. Haga, H.; Garland, C.W. Calorimetric study of heptyloxybenzylidene butylaniline in silica aerogels. *Liq. Cryst.* **1997**, *22*, 275–277.

13. Haga, H.; Garland, C.W. Effect of silica aerosil particles on liquid-crystal phase transitions. *Phys. Rev. E* **1997**, *56*, 3044–3052.

14. Haga, H.; Garland, C.W. Thermal study of the influence of aerosils on the phase transitions of heptyloxybenzylidene butylaniline. *Liq. Cryst.* **1997**, *23*, 644–652.

15. Qian, S.; Iannacchione, G.S.; Finotello, D. Critical behavior of a smectic-A to nematic phase transition imbedded in a random network of voids. *Phy. Rev. E* **1998**, *57*, 4305–4315.

16. Iannacchione, G.S.; Garland, C.W.; Mang, J.T.; Rieker, T.P. Calorimetric and small angle X-ray scattering study of phase transitions in octylcyanobiphenyl-aerosil dispersions. *Phy. Rev. E* **1998**, *58*, 5966–5981.

17. Busch, K.; John, S. Liquid-crystal photonic-band-gap materials: The tunable electromagnetic vacuum. *Phys. Rev. Lett.* **1999**, *83*, 967–970.

18. Yablonovitch, E. Liquid *vs.* photonic crystals. *Nature* **1999**, *401*, 539–541.

19. Wiersma, D.S.; Cavalieri, S. Light emission-A temperature-tunable random laser. *Nature* **2001**, *414*, 708–709.

20. Gottardo, S.; Wiersma, D.S.; Vos, W.L. Liquid crystal infiltration of complex dielectrics. *Phys. B* **2003**, *338*, 143–148.

21. Caggioni, M.; Roshi, A.; Barjani, S.; Mantegazza, F.; Iannacchione, G.S.; Bellini, T. Isotropic to nematic transition os aerosil-disordered liquid crystals. *Phys. Rev. Lett.* **2004**, *93*, 127801:1–127801:4.

22. Cordoyiannis, G.; Nounesis, G.; Bobnar, V.; Kralj, S.; Kutnjak, Z. Confinement-induced orientational order in a ferroelectric liquid crystal containing dispersed aerosils. *Phys. Rev. Lett.* **2005**, *94*, 027801:1–027801:4.

23. Mercuri, F.; Paolini, S.; Zammit, U.; Marinelli, M. Dynamics at the nematic-isotropic phase transition in aerosil dispersed liquid crystal. *Phys. Rev. Lett.* **2005**, *95*, 247801:1–247801:4.

24. Diez, S.; López, D.O.; de la Fuente, M.R.; Pérez-Jubindo, M.A.; Salud, J.; Tamarit, J.L. Thermodynamic and dielectric studies concerning the influence of cylindrical submicrometer confinement on heptyloxycyanobiphenyl. *J. Phys. Chem. B* **2005**, *109*, 23209–23217.

25. Diez, S.; Pérez-Jubindo, M.A.; de la Fuente, M.R.; López, D.O.; Salud, J.; Tamarit, J.L. On the influence of cylindrical sub-micrometer confinement on heptyloxycyanobiphenyl (7OCB). A dynamic dielectric study. *Chem. Phys. Lett.* **2006**, *423*, 463–469.

26. Diez, S.; Pérez-Jubindo, M.A.; de la Fuente, M.R.; López, D.O.; Salud, J.; Tamarit, J.L. Dielectric relaxation in bulk and cylindrically confined octylcyanobiphenyl (8CB). *Liq. Cryst.* **2006**, *33*, 1083–1091.

27. Kralj, S.; Cordoyiannis, G.; Zidansek, A.; Lahajnar, G.; Amenitsch, H.; Zumer, S.; Kutnjak, Z. Presmectic wetting and supercritical-like phase behavior of octylcyanobiphenyl liquid crystal confined to controlled-pore glass matrices. *J. Chem. Phys.* **2007**, *127*, 154905:1–154905:9.

28. Perez-Jubindo, M.A.; de la Fuente, M.R.; Diez-Berart, S.; Lopez, D.O.; Salud, J. Influence of cylindrical submicrometer confinement on the static and dynamic properties in nonyloxycyanobiphenyl (9OCB). *J. Phys. Chem. B* **2008**, *112*, 6567–6577.

29. Cordoyiannis, G.; Kurihara, L.K.; Martinez-Miranda, L.J.; Glorieux, C.; Thoen, J. Effects of magnetic nanoparticles with different surface coating on the phase transitions of octylcyanobiphenyl liquid crystal. *Phys. Rev. E* **2009**, *79*, 011702:1–011702:5.

30. De Luca, A.; Barna, V.; Ferjani, S.; Caputo, R.; Versace, C.; Scaramuzza, N.; Bartolino, R.; Umeton, C.; Strangi, G. Laser action in dye doped liquid crystals: From periodic structures to random media. *J. Nonlinear Opt. Phys.* **2009**, *18*, 349–365.

31. De la Fuente, M.R.; Lopez, D.O.; Perez-Jubindo, M.A.; Dunmur, D.A.; Diez-Berart, S.; Salud, J. Cylindrical sub-micrometer confinement results for the odd-symmetric dimer α,ω-bis[(4-cyanobiphenyl)-4′yloxy]undecane (BCB.O11). *J. Phys. Chem. B* **2010**, *114*, 7864–7873.

32. Karatairi, E.; Rozic, B.; Kutnjak, Z.; Tzitzios, V.; Nounesis, G.; Cordoyiannis, G.; Thoen, J.; Glorieux, C.; Kralj, S. Nanoparticle-induced widening of the temperature range of liquid-crystalline blue phases. *Phys. Rev. E* **2010**, *81*, 041703:1–041703:5.

33. Diez-Berart, S.; Lopez, D.O.; de la Fuente, M.R.; Salud, J.; Perez-Jubindo, M.A.; Finotello, D. Critical behaviour in liquid-crystalline phase transitions: A comparative study of 9OCB in bulk and Anopore membranes. *Liq. Cryst.* **2010**, *37*, 893–901.

34. Grigoriadis, C.; Duran, H.; Steinhart, M.; Kappl, M.; Butt, H.J.; Floudas, G. Suppression of phase transitions in a confined rodlike liquid crystal. *ACS Nano* **2011**, *5*, 9208–9215.

35. Joshi, T.; Prakash, J.; Kumar, A.; Gangwar, J.; Srivastava, A.K.; Singh, S.; Biradar, A.M. Alumina nanoparticles find an application to reduce the ionic effects of ferroelectric liquid crystal. *J. Phys. D* **2011**, *44*, 315404:1–315404:7.

36. Kralj, S.; Cordoyiannis, G.; Jesenek, D.; Zidansek, A.; Lahajnar, G.; Novak, N.; Amenitsch, H.; Kutnjak, Z. Dimensional crossover and scaling behavior of a smectic liquid crystal confined to controlled-pore glass matrices. *Soft Matter* **2012**, *8*, 2460–2470.

37. Zupancic, B.; Diez-Berart, S.; Finotello, D.; Lavrentovich, O.D.; Zalar, B. Photoisomerization-controlled phase segregation in a submicron confined azonematic liquid crystal. *Phys. Rev. Lett.* **2012**, *108*, 257801:1–257801:5.

38. Stine, K.J.; Garland, C.W. Calorimetric study of nematic to smectic-A tricritical behavior. *Phys. Rev. A* **1989**, *39*, 3148–3156.

39. Salud, J.; Lopez, D.O.; Diez-Berart, S.; de la Fuente, M.R. Tests of the tricritical point in the SmA-to-N phase transition of binary mixtures of butyloxybenzylidene octylaniline and hexyloxybenzylidene octylaniline. *Liq. Cryst.* **2013**, *40*, 293–304.

40. Diez-Berart, S.[1]; López, D.O.[1]; Salud, J.[1]; Sebastián, N.[2]; Robles-Hernández, B.[2]; De la Fuente, M.R.[2]; Diego, J.A.[3]; Sellarés, J.[3]; Ros, M.B[4]. [1]GRPFM, Departament de Física i Enginyeria Nuclear, E.T.S.E.I.B., Universitat Politècnica de Catalunya, Barcelona, Spain; [2]Departamento de Física Aplicada II, Facultad de Ciencia y Tecnología, Universidad del País Vasco (UPV/EHU), Bilbao, Spain; [3]DILAB, Departament de Física i Enginyeria Nuclear, E.T.S.E.I.B., Universitat Politècnica de Catalunya, Barcelona, Spain; [4]Departamento de Química Orgánica, Universidad de Zaragoza, Instituto de Ciencia de Materiales de Aragón (ICMA-CSIC), Zaragoza, Spain. Unpublished work, 2014.

41. Dunmur, D.A.; Toriyama, K. Dielectric Properties. In *Physical Properties of Liquid Crystals*, 1st ed.; Demus, D., Goodby, J.W., Gray, G.W., Spiess, H.W., Eds.; Wiley-VCH: Weinheim, Germany, 1999; pp. 129–150.

42. Nordio, P.L.; Rigatti, G.; Segre, U. Dielectric relaxation theory in nematic liquids. *Mol. Phys.* **1973**, *25*, 129–136.

43. Cusmin, P.; de la Fuente, M.R.; Salud, J.; Pérez-Jubindo, M.A.; Diez-Berart, S.; López, D.O. Critical behavior and scaling relationships at ehe SmA$_d$-N and N-I transitions in nonyloxycyanobiphenyl (9OCB). *J. Phys. Chem. B* **2007**, *111*, 8974–8984.

44. Salud, J.; Cusmin, P.; de la Fuente, M.R.; Pérez-Jubindo, M.A.; López, D.O.; Diez-Berart, S. Study of the critical behavior and scaling relationships at the N-to-I phase transition in hexyloxycyanobiphenyl. *J. Phys. Chem. B* **2009**, *113*, 15967–15974.

45. Puertas, R.; Rute, M.A.; Salud, J.; López, D.O.; Diez, S.; van Miltenburg, J.C.; Pardo, L.C.; Tamarit, J.L.; Barrio, M.; Pérez-Jubindo, M.A.; de la Fuente, M.R. Thermodynamic, crystallographic and dielectric study of the nature of glass transitions in cyclo-octanol. *Phys. Rev. B* **2004**, *69*, 224202:1–224202:9.

46. Sebastián, N.; de la Fuente, M.R.; Lopez, D.O.; Perez-Jubindo, M.A.; Salud, J.; Diez-Berart, S.; Ros, M.B. Dielectric and thermodynamic study on the liquid crystal dimer α-(4-cyanobiphenyl)-4′-oxy)-ω-(1-pyreniminebenzylidene-4′-oxy)undecane (CBO11O.Py). *J. Phys. Chem. B* **2011**, *115*, 9766–9775.